Residue length and solvation model dependency of elastinlike polypeptides

Mustafa Bilsel* and Handan Arkin†
Department of Physics Engineering, Ankara University, Tandoğan, Ankara 06100, Turkey
(Received 11 February 2010; published 6 May 2010)

We have performed exhaustive multicanonical Monte Carlo simulations of elastinlike polypeptides with a chain including amino acids (valine-proline-glycine-valine-glycine)$_n$ or in short $(VPGVG)_n$, where n changes from 1 to 4, in order to investigate the thermodynamic and structural properties. To predict the characteristic secondary structure motifs of the molecules, Ramachandran plots were prepared and analyzed as well. In these studies, we utilized a realistic model where the interactions between all types of atoms were taken into account. Effects of solvation were also simulated by using an implicit-solvent model with two commonly used solvation parameter sets and compared with the vacuum case.

DOI: 10.1103/PhysRevE.81.051906 PACS number(s): 87.15.−v, 87.15.A−, 05.10.−a, 87.15.Cc

I. INTRODUCTION

Protein folding is one of the most intensively studied and still unsolved problems in biology. The process by which a protein folds into its biologically active state cannot be traced in all details solely by experiments. Therefore, many theoretical and experimental studies focus on determination of the three-dimensional structure of these molecules. Recently, molecular modeling has attracted considerable attention for applications in designing and fabrication of nanostructures leading to the development of advanced materials. In a newly growing field of research, synthetic peptides are investigated for their use in nanodevices, by exploiting their self-assembly properties [1,2]. The self-assembly of biomolecular building blocks plays an increasingly important role in the discovery of new materials, with a wide range of applications in nanotechnology and medical technologies such as drug delivery systems [3]. In these studies, several types of biomaterials are developed, ranging from models for studying protein folding to molecular materials for producing peptide nanofibers and peptide surfactants by designing various classes of self-assembling peptides [4]. These experiments reveal many different interesting and important problems, which are related to general aspects of the questions of why and how proteins fold. In this context, modern simulation techniques have opened another window to give a new insight to protein folding problem [5,6].

In this paper, structural properties of peptides (valine-proline-glycine-valine-glycine)$_n$ or in short $(VPGVG)_n$ known as elastinlike polypeptides (ELPs) have been investigated. Generally, in the simulated sequences, the ELPs are important in tissue engineering so they arouse interest due to some of their important and attractive properties. One of the most important properties is the self-assembling potential. Because of the self-assembling property, ELPs are fairly convenient for the production of microtubes and nanotubes. Other biomaterials produced from ELPs are hydrogels [7], plates [8], nanoparticles [9], spongelike isotropic networks [10], and nanoporous materials [11]. ELPs are not soluble in water and are the most stable proteins with 70-year half-life [12].

ELPs are a member of polypeptides derived from a portion of the primary sequence of elastin, valine-proline-glycine-*X*-glycine (*VPGXG*) pentapeptide, where *V* is valine, *P* is proline, *G* is glycine, and *X* is any amino acid except proline. Several studies have explored the effect of substituting different amino acids in the fourth position of the sequence on thermally responsive behavior. ELPs and their derivatives have been used for a number of applications, including drug delivery, protein purification, and tissue engineering. For example, Chilkoti and coworkers have evaluated temperature-responsive ELPs for potential applications in cancer therapy [13,14].

In previous works, x-ray diffraction data were used to determine, at room temperature, the crystal structure of a repeat pentapeptide of elastin [15]. Nuclear magnetic resonance (NMR) studies have shown that the repeated-oligopeptide segments of elastin are composed of subunits that are conformationally equivalent within the NMR time scale. Several secondary structural elements have been proposed as features of one or more of these repeated peptide segments [16]. Alternative approaches such as computer molecular modeling starting from amino acid sequences can contribute to a better understanding of the three-dimensional structures of these repeating oligopeptides [17].

Our present study includes (1) Simulations to understand the change in structural properties when it is progressed from *VPGVG* to $(VPGVG)_2$, $(VPGVG)_3$, and $(VPGVG)_4$ chains in a solvation model. (2) Simulations of $(VPGVG)_2$ carried out in vacuum and two different solvation models to comprehend the effect of solvation models on structural properties of ELPs.

From a computational point of view, the difficulties arise from the complex form of forces within the molecules. The atomic interactions of a protein are commonly modeled by an empirical potential-energy function, which typically leads to a complex energy landscape consisting of a tremendous number of local minima.

Due to the local minima levels separated by high-energy barriers, it is difficult to find global minimum in energy map of the molecules. The development of novel global optimization algorithms for protein folding problem is still an active area of research. To overcome this problem, we perform

*mfbilsel@gmail.com
†handan.olgar@eng.ankara.edu.tr

simulations in a generalized ensemble [18,19] where each state is weighted by a non-Boltzmann probability weight factor, so that a flat histogram in potential-energy space may be realized. This allows the simulation to escape from any energy barrier and to sample much wider conformational space than conventional methods. One of the well-known powerful generalized-ensemble methods is the multicanonical (MUCA) simulation method [20]. The trapping problem can be alleviated by the MUCA method. Furthermore, it creates another advantage that allows the calculation of various thermodynamic quantities as functions of temperature from one simulation run. Employing multicanonical Monte Carlo (MC) sampling, from one simulation run, we analyze the global minimum-energy structures and illuminate the thermodynamic and structural properties of these peptides and determine *all* the thermodynamically stable conformations populated by the molecule, not only the stable structure at room temperature. These techniques applied to all-atom descriptions of proteins have been very successful in the past, e.g., in revealing the statistical mechanics in the folding process of small proteins [17,21–23]. For sequences with more than 50 residues, studies of thermodynamic and kinetics employing realistic physical models are computationally demanding [24] and an alternative would be coarse-grained off-lattice models, which allow for systematic thermodynamic study [25,26].

II. SIMULATION METHOD

In these respects, we have used multicanonical algorithm while modeling ELPs. To understand the basis of the MUCA method, it should be first reminded the usual metropolis MC method in the canonical ensemble samples with the Boltzmann probability density,

$$P^B(x) = e^{[-E/k_BT]/Z}, \tag{1}$$

where x labels the configuration, T is the absolute temperature, k_B is the Boltzmann constant, and Z is the partition function. Thus, the probability of the energy E is

$$P_T^B(E) = n(E)e^{[-E/k_BT]/Z}, \tag{2}$$

where $n(E)$ is the density of states. A canonical MC simulation at T spans a narrow range of energies. The MUCA ensemble, on the other hand, is based on a probability function in which the different energies are equally probable,

$$P^{MU}(E) \sim n(E)\omega(E) = \text{const}, \tag{3}$$

where $\omega(E)$ stands for multicanonical weight factors; hence, a one-dimensional random walk in the energy space may result. However, the implementation of MUCA is not straightforward because the density of states is unknown *a priori*. Therefore, a recursion procedure [20] is used: we first divide the energy range into $L-2$ equal segments i defined by $[E_{i-1}, E_i]$, where

$$E_i - E_{i-1} = \Delta Ei > 0 \quad \text{for } i = 2, \ldots, L-1, \tag{4}$$

with

$$E_0 = -\infty, \quad E_L = +\infty. \tag{5}$$

The definition of our parametrization of the MUCA weights reads

$$\omega_i(x) = e^{(-b_iE_x+a_i)} \quad \text{for } E_{i-1} < E_x \leq E_i, \tag{6}$$

where the b_i values are inverse microcanonical temperatures, $b_i = 1/k_BT_i$, and a_i follow from the temperature coefficients b_i by enforcing continuity of $S(E)$ known as microcanonical entropy at the border energies between the intervals,

$$S_i(E_{i-1}) = S_{i-1}(E_{i-1}) \Rightarrow a_{i-1} = a_i + (b_{i-1} - b_i)E_{i-1}. \tag{7}$$

It remains to determine b_i by recursive simulations. This is done in the following way: after the $(m-1)$th simulation, the ω_{m-1}^i functions become known and define a probability distribution according to the mth simulation. The multicanonical parameter b_{i-1}^m in the mth step reads

$$b_{i-1}^m = b_{i-1}^{m-1} + g_{i-1}^m \ln[H_{i-1}^m/H_i^m]/\Delta E_i, \tag{8}$$

where H_i^m denotes the histogram entry and g_{i-1}^m is a statistical weight evaluated from the histograms of all previous recursion simulations. The iterative procedure is followed by a long production run based on the fixed weight factors where equilibrium configurations are sampled. Hence, a simulation with this weight factor, which has no temperature dependence, generates a one-dimensional random walk in the energy space, allowing itself to escape from being trapped in any energy local minimum. Reweighting techniques [27] enable one to obtain Boltzmann averages of various thermodynamic properties over a large range of temperatures. The advantage of this algorithm lies in the fact that it not only alleviates the multiple-minima problem but also allows the calculation of various thermodynamic quantities as functions of temperature from one simulation run. This demonstrates the superiority of the method.

III. MODEL

In the simulations, a peptide is modeled with all of its atoms. Each atom i, located at the position r_i, carries a partial charge q_i. Covalent bonds between atoms, according to the chemical structure of the amino acids, are considered rigid, i.e., bond lengths are kept constant, as well as bond angles between covalent bonds and certain rigid torsion angles. Distances between no bonded atoms i and j are defined as $r_{ij} = |r_i - r_j|$ and measured in Å. Each unit can rotate around two such bonds: the C_α-C' and the N-C_α bonds. The rotation around the N-C_α bond is denoted by the φ angles and the rotation around the C_α-C' bond is denoted by the ψ angles. The side chain angles are denoted by χ. The peptide bond angles ω are kept fixed at 180° to their common value. The atomic composition of the peptide backbone and dihedral angles are shown in Fig. 1.

The sequences are modeled by the well-known potential-energy function ECEPP/3 [28–31] (empirical conformational energies for proteins and polypeptides) which is given by the sum of the electrostatic term, 12-6 Lennard-Jones term, and the hydrogen bond term for all pairs of atoms in the peptide together with the torsion term for all torsion angles,

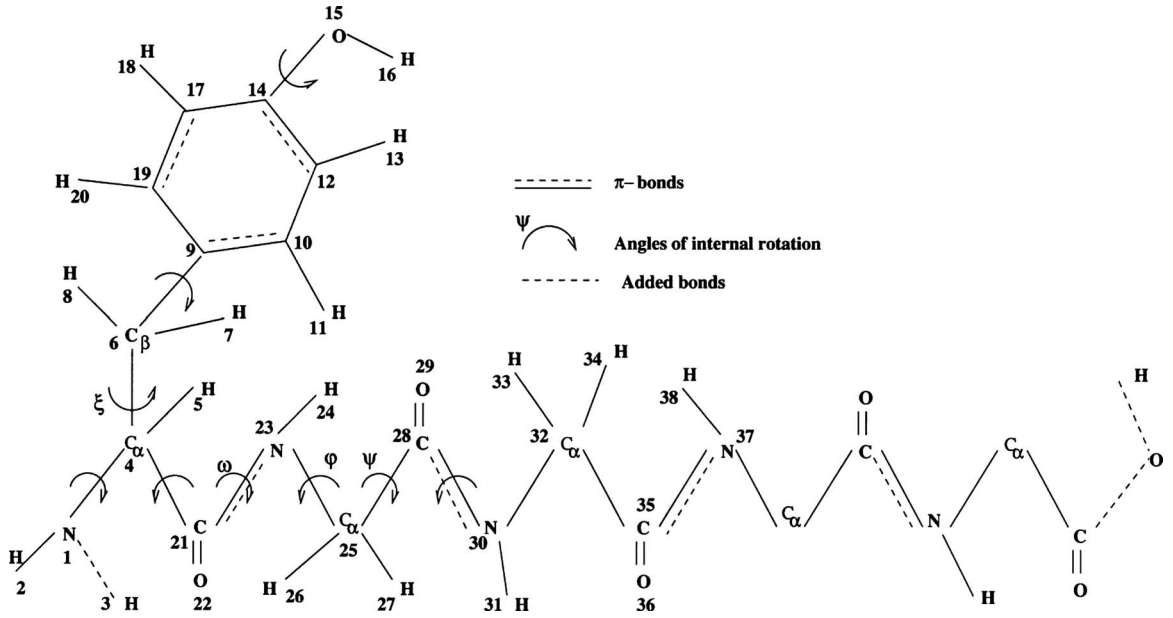

FIG. 1. Atomic composition of the peptide backbone and dihedral angles.

$$E_{ECEPP/3} = E_{LJ} + E_{el} + E_{hb} + E_{tor}, \tag{9}$$

$$E_{LJ} = \sum_{j>i} \left(\frac{A_{ij}}{r_{ij}^{12}} \right) - \left(\frac{B}{r_{ij}^{6}} \right), \tag{10}$$

$$E_{el} = \sum_{j>i} \frac{q_i q_j}{\varepsilon r_{ij}}, \tag{11}$$

$$E_{hb} = \sum_{j>i} \left(\frac{C_{ij}}{r_{ij}^{12}} \right) - \left(\frac{D_{ij}}{r_{ij}^{10}} \right), \tag{12}$$

$$E_{tor} = \sum_{n} U_n [1 \pm \cos(k_n \varphi_n)], \tag{13}$$

where r_{ij} is the distance between the atoms i and j, ξ_l is the lth torsion angle, and energies are measured in kcal/mol. In all simulations, the electrostatic permittivity in the protein interior is to be $\varepsilon=2$ (its common value in ECEPP simulations). For example, a conformation of $(VPGVG)_4$ sequence is defined by 60 degrees of freedom, the 36 backbone dihedral angles ϕ and ψ, and the 24 side chain dihedral angles χ. The angle pairs ϕ and ψ of each residue are usually plotted against each other in Ramachandran plots, which display the distribution of angles. In all simulations, NH_2 and COOH were chosen as the N- and C-terminal groups, respectively. Proline's ϕ is considered rigid at $-68.8°$. We always used the trans-down-puckering conformation of the proline ring. For the implicit-solvent simulations, the model is extended by the solvation-energy contribution, which is given by [32]

$$E_{solv} = \sum_{i} \sigma_i A_i, \tag{14}$$

where A_i is the solvent-accessible surface area of the ith atom for a given conformation and σ_i is the solvation parameter for the ith atom. The values for σ_i depend on the type of the ith atom and are parametrized according to the Ref. [33] (SCH2 solvation model) and Ref. [34] (OONS solvation model). In this approximation, one assumes that the free-energy difference between atomic groups immersed in the protein interior and groups exposed to water is proportional to the solvent accessible surface area A_i of the ith atom with the parameters σ_i, which are experimentally determined proportionality factors. The described peptide model and the force field are implemented into the software package simple molecular mechanics for proteins (SMMP) [35], which are used in this study.

IV. RESULTS AND DISCUSSION

The implementation of MUCA is not straightforward as the density of states $n(E)$ is unknown *a priori*. Therefore, the multicanonical weights have to be determined in the first stage of the simulation process by an iterative procedure until the histogram is "flat" in the desired energy interval. We note that the efficiency of the determination of the multicanonical weights usually depends on the choice of the simulation temperature, which is in present study $T_{sim}=1000$ K. The reason is that, since the "flat" energy histogram covers a larger region in subsequent recursions, energetic states are hit for the first time, where the multicanonical weights are still undetermined. Because the ratio of the weights controls the acceptance of an update, the dynamics of the recursion part of the algorithm is influenced. This can be "smoothed" by a carefully choice of simulation temperature.

In our implementation, we first carried out canonical (i.e., constant T) MC simulations at relatively high temperatures and MUCA test runs, which enabled us to determine the required energy ranges. Then we performed full MUCA simulations, which cover reliably the high-temperature region up to $T_{sim}=1000$ K. In these simulations the energy range, for example, for sequence $(VPGVG)_2$ is [30,

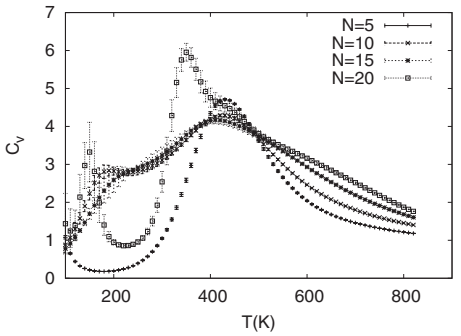

FIG. 2. The specific heat as a function of temperature for polypeptides with $N=5$, 10, 15, and 20 residues in solvent (SCH2).

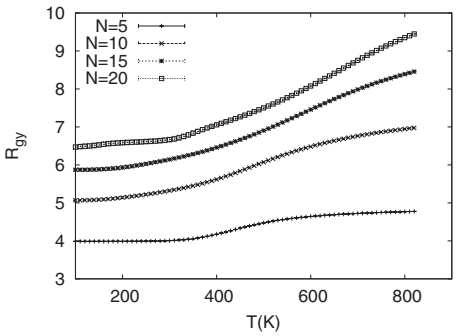

FIG. 3. R_{gy} as a function of temperature for polypeptides with $N=5$, 10, 15, and 20 residues in solvent (SCH2).

$-25]$ kcal/mol which was divided into 56 bins of 1 kcal/mol each. For $(VPGVG)_4$ the range is $[50,-50]$ kcal/mol and was divided into 101 bins, that is, the binning is related with the length of the sequence.

At each update step, a single dihedral angle whose trial value was obtained at random within the range $[-180°,180°]$ was treated. As an example introduced in the paper, for the sequence $(VPGVG)_4$ 60 dihedral angles were visited in a predefined order going from first residue to last, where such a cycle of n MC steps ($n=60$) defines a sweep. The weights were built in about 25 recursions during a long single simulation, where the multicanonical parameters were iterated every 8000–30 000 sweeps ranging from smaller molecule to greater molecule. Additionally, protein-solvent interaction energy included model demands more CPU time, that is, the multicanonical parameters were iterated 15 000 sweeps for $(VPGVG)_2$ peptide in vacuum and 21 000 sweeps for implicit-solvent model. Then, we performed a full simulation of $2-5\times10^6$ sweeps with fixed weights, which covers the temperature region up to $T_{max}=1000$ K reliably. From the MUCA production run canonical expectation values of thermodynamic quantities were obtained by reweighting [27]. The statistical errors were estimated with the standard Jackknife technique [36,37].

In the first part of our work, $VPGVG$, $(VPGVG)_2$, $(VPGVG)_3$, and $(VPGVG)_4$ polypeptides have been studied in a solvent called SCH2 to realize the effect of residue increase on conformational transition. Henceforth residue numbers are increased from 5 to 20 and from now on sometimes we call polypeptide names as $N=5$, 10, 15, and 20. For polymers or peptides, the crossover between such microstates is accompanied by a cooperative conformational transition. Thus, it is reasonable to compare the behavior of different sequences with regard to energetic fluctuations, the specific heat (in unit of R)

$$C_v = \frac{1}{(RT)^2}(\langle E^2\rangle - \langle E\rangle^2). \tag{15}$$

Near the peak temperatures, the peptide exhibits conformational activity. In Fig. 2 the specific heat as a function of temperature is plotted to determine the transition temperatures for the residue numbers $N=5$, 10, 15, and 20. Related conformational transition temperatures for residues $N=5$, 10, 15, and 20 are depicted from the specific heat curves and are 435, 425, 410, and 350 K, respectively. Increasing residue number decreases conformational transition temperatures of the polypeptides. Obtained inverse relation between residue number and conformational transition temperature is consistent with experimental results [38] in which it is stated that increasing residue number increases molecular weight but decreases conformational transition temperature. One important point, as seen in the figure, is that for the peptide $N=5$ the specific heat curve has only one pronounced peak which means that the peptide has a two-state folding channel. The protein changes from an unstructured extended configuration above the specific heat peak to a compact one with secondary structure below the specific heat peak. When we increase the residue length for $N=10$ and 15, there appears a shoulder in the specific heat, which signals intermediate states in the folding channel. Finally, in $N=20$ a second peak comes into being, which points that the folding is a two-step process [39,40]. First, the protein changes from random unstructured conformations to highly ordered secondary structures and then in the second step the native state is selected out from the ensemble of compact configurations with synchronous formation of secondary structure [41].

We have also calculated the radius of gyration R_{gy}, as a rather global quantity, which is mainly useful for identifying the structural collapse caused by a conformational transition. However, for determining highly ordered secondary structures, the radius of gyration is too rough to measure and is therefore of less importance for the understanding of secondary structure formation [42,43]. In Fig. 3 the R_{gy} as a function of temperature is shown for the sequences $N=5$, 10, 15, and 20. R_{gy} is proportional to temperature; it decreases at low temperatures and increases at high temperatures. The radius of gyration values of polypeptides increase with residue number, that is, the highest value is obtained for $N=20$.

In order to check the secondary structures, the distribution of ϕ and ψ dihedral angles of polypeptides with different residue lengths at room temperature 300 ± 10 K is analyzed by Ramachandran plots, which estimate the secondary structure of polypeptides. There are various experimental methods (spectroscopic, viscosimetric, microscopic, etc.) used to recognize the secondary structure formation. These methods give an indication of conformations dominant in the structure of a protein. On the other hand, MUCA is the most important as being a thermodynamic method that enables simulating a system over a large range of temperatures. This aspect is

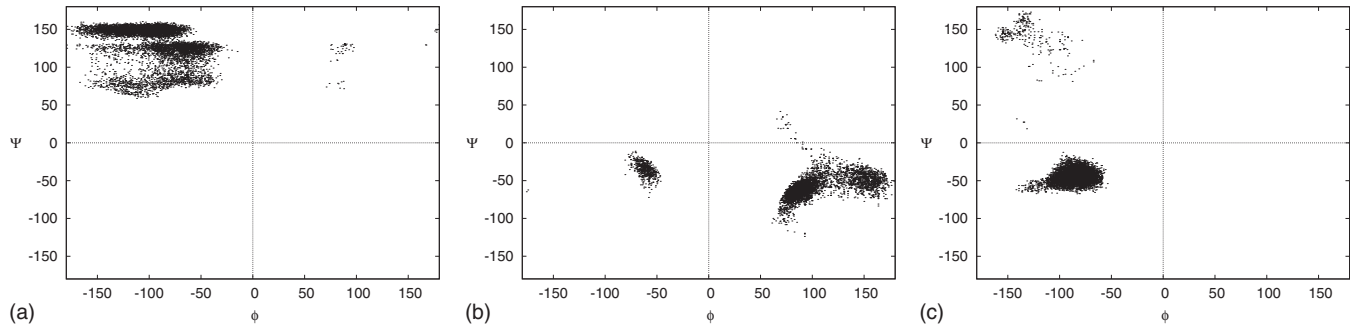

FIG. 4. Ramachandran plot for *VPGVG* at $T=300\pm10$ K in solvent (SCH2).

used to prepare Ramachandran plots, which provide the distributions of the dihedral angles and allow distinguishing different types of highly ordered segments. Ramachandran plot in Fig. 4 describes *VPGVG* polypeptide for Val1, Gly3, and Val4 amino acids. To be able to compare simulation results with experimental ones, room temperature is chosen.

When Ramachandran plots are analyzed, it is observed that βII turn is the dominant structure between Val1-Pro2 and Gly3-Val4-Gly5 bridges except for Pro2-Gly3 bridge. βII turn has characteristics dihedral angle set $(\phi,\psi)=(-60,120)$. These results are in agreement with previous studies, both experimental [44] and simulation [45] approaches, which suggest that main secondary structure in elastin is short β turns. Circular dichroism (CD) and NMR measurements gave evidence of flexible β turns as the dominant structural feature [46,47]. In addition, the literature on protein structure indicates that the occurrence of high-probability β turns in proline at the second and glycine at the third position is consistent with the results of the present study [48].

Ramachandran plot in Fig. 5 is plotted to determine the secondary structure of $(VPGVG)_2$ polypeptide. $(VPGVG)_2$ polypeptide obtained by increasing the residue number of *VPGVG* has higher order βII turns in its secondary structure. Formation of βII turns has been observed in all residue bridges.

Ramachandran graphs for $(VPGVG)_3$ and $(VPGVG)_4$ polypeptides have been plotted and similarity with $(VPGVG)_2$ is observed so graphs are not included herein. βII turn is the dominant structure both in $(VPGVG)_3$ and $(VPGVG)_4$ polypeptides and its content increases when compared with $(VPGVG)_2$. In Figs. 6(a) and 6(b), the global minimum-energy conformations of these sequences are given. The $(VPGVG)_3$ structure has three β turn bridges and also some β-strand motifs. On the other hand, the sequence $(VPGVG)_4$ has more turns (four turn bridges) and more strand motifs. In this type of peptides β structures (turns, sheets, and strands) are more probable because in the presence of water the Gly residue behaves as a helix breaker. Therefore, the structures consist of high level of β structures, particularly β turns. In the second part of our study, to see the effects of solvation on conformational transition, we have

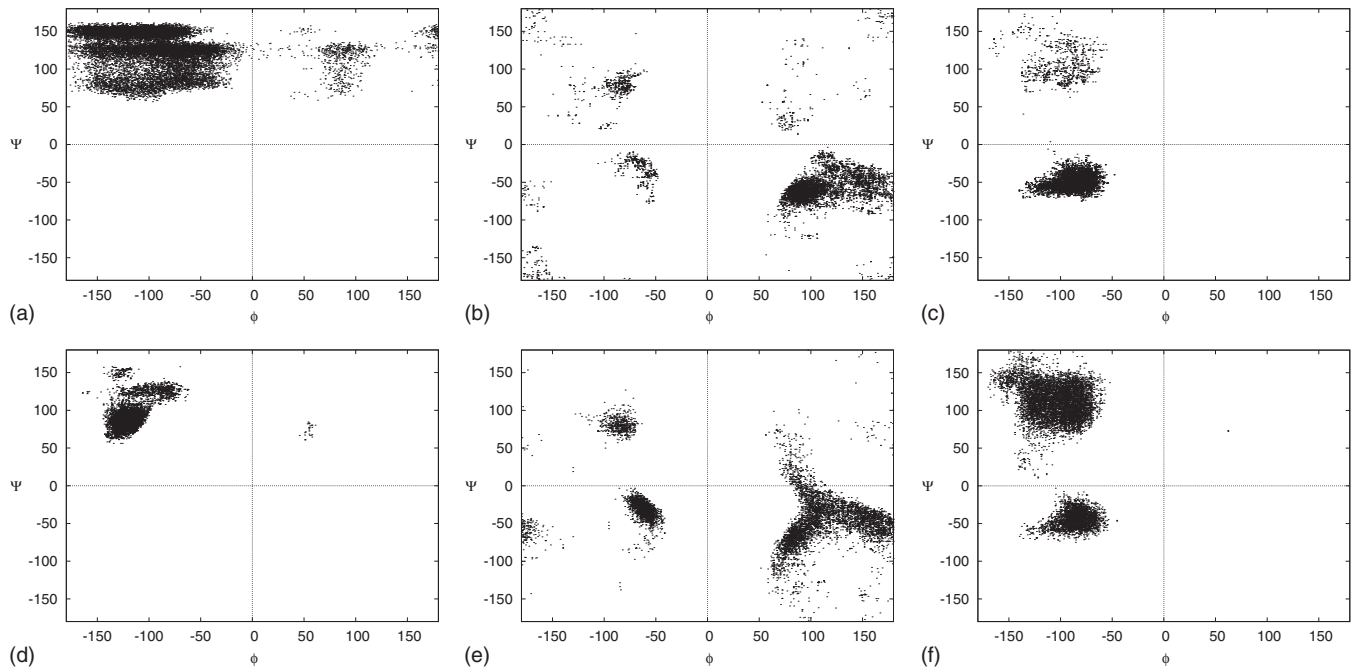

FIG. 5. Ramachandran plot for $(VPGVG)_2$ at $T=300\pm10$ K in solvent (SCH2).

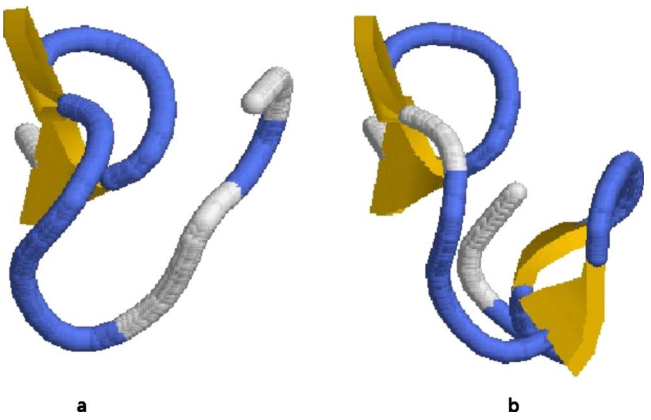

FIG. 6. (Color online) Global minimum-energy conformations of sequences (a) $(VPGVG)_3$ and (b) $(VPGVG)_4$ in solvent (SCH2).

simulated the $(VPGVG)_2$ polypeptide in vacuum and two commonly used surface-accessible area solvent models OONS [34] and SCH2 [20].

In Fig. 7 specific heat as a function of temperature for $(VPGVG)_2$ polypeptide is indicated. Transition temperatures in vacuum, SCH2, and OONS are 470, 425, and 380 K, respectively. As seen in the figure, the main effect of the solvent is the strengthening of the conformational transition (the pronounced peak in the specific heat curves) which is also present in the vacuum case. Furthermore, the transition temperature is shifted by about 55–90 K toward lower temperatures. These results are as expected, since it is known that solvent stabilizes secondary structures and therefore the barrier to resolve the ordered secondary structures is higher than in the vacuum case, and the relaxation of the fluctuations of the peptide-solvent coupling degrees of freedom leads to a lower transition temperature.

The radius of gyration as a function of temperature is plotted in Fig. 8. While radius R_{gy} decreases at low temperatures, it increases at high temperatures. The radius of gyration values change in a small interval $R_{gy} \approx 5-7.5$ Å, so the radius of gyration cannot be used as a decisive parameter to recognize the compactness of polypeptides.

We have also analyzed the Ramachandran plots for different solvation models and compared them with the vacuum case at 300 K, but there is no effect on secondary structure (data not shown). Only the conformational transition temperature changes for different solvation parameter sets. Because as it is seen from specific heat curves, the transition from unstructured configurations to secondary structure is at higher temperature than 300 K. Therefore, at 300 K the secondary structures are formed for all the cases.

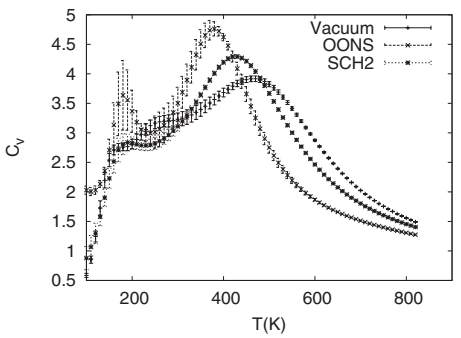

FIG. 7. The specific heat as a function of temperature for $(VPGVG)_2$ polypeptide.

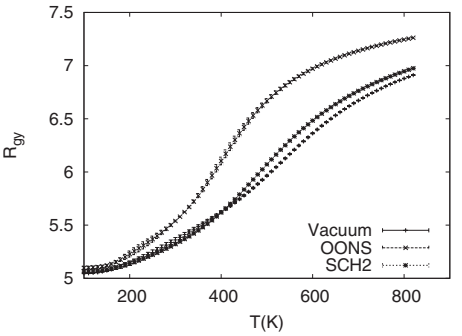

FIG. 8. Radius of gyration R_{gy} as a function of temperature for $(VPGVG)_2$ polypeptide.

Finally, we have also compared the global minimum-energy conformations of the sequence $(VPGVG)_2$ in vacuum and two commonly used surface accessible area solvent models by aligning the conformations and calculating the root-mean-square distance (RMSD) parameter. In Fig. 9, the three overlapped global minimum-energy conformations for different situations are given. By taking only backbone into account and vacuum conformation as reference configuration, the calculated RMSD values for SCH2 and OONS models are 0.898 and 0.538, respectively. When all the atoms are taken into account, the RMSD values differ slightly from 1.055 to 0.822, respectively. All the three conformations have two β-turn bridges as secondary structure motifs. As a result, we can conclude that the solvation lowers the transition temperatures and strengthens only the transition, but has no significant effect on the secondary structure motifs. Thus, the global minimum-energy conformation bears the same secondary structure motifs.

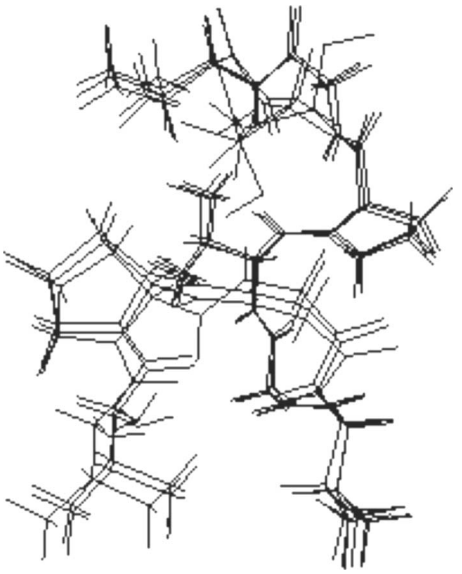

FIG. 9. The aligned global minimum-energy conformations of vacuum, SCH2, and OONS simulations

V. CONCLUSION

We have analyzed thermodynamic properties and secondary structure motifs for the sequences *VPGVG*, $(VPGVG)_2$, $(VPGVG)_3$, and $(VPGVG)_4$ of ELPs. Employing an all-atom model based on the ECEPP/3 force field with different implicit solvation parameter sets and applying the implementation of the multicanonical Monte Carlo method in the SMMP package, we found that βII turn is the dominant structure between Val1-Pro2 and Gly3-Val4-Gly5 bridges except for Pro2-Gly3 bridge. These results are in agreement with previous studies, both experimental [44] and simulation [45] approaches, which suggest that main secondary structure in elastin is short β turns. CD and NMR measurements gave evidence of flexible β turns as the dominant structural feature [46,47]. In order to determine the solvent effects on the sequences, we have also extended our simulations with the two commonly used solvation parameter sets. Solvation causes the transition to occur at lower temperatures and strengthens the transition, but different solvation parameter sets result in different temperatures. Therefore, we expect that by generating reasonable environmental conditions, the secondary structure formation could happen as intended. This is an important issue since it is generally expected that selective synthetic peptides and polymers may play an important role in future nanotechnological applications.

ACKNOWLEDGMENTS

H.A. acknowledges support by The Scientific and Technological Research Council of Turkey under Project No. 104T150 and The Turkish Academy of Sciences under the program to Reward Successful Young Scientists.

[1] S. Santoso, W. Hwang, H. Hartman, and S. Zhang, Nano Lett. **2**, 687 (2002).
[2] S. Vauthey, S. Santosa, H. Gong, N. Watson, and S. Zhang, Proc. Natl. Acad. Sci. U.S.A. **99**, 5355 (2002).
[3] J. A. Hubbell, Curr. Opin. Biotechnol. **10**, 123 (1999).
[4] T. Holmes, S. De Lacella, X. Su, A. Rich, and S. Zhang, Proc. Natl. Acad. Sci. U.S.A. **97**, 6728 (2000).
[5] H. Arkin and T. Çelik, Int. J. Mod. Phys. C **14**, 985 (2003).
[6] G. Gökoğlu, M. Bachmann, T. Çelik, and W. Janke, Phys. Rev. E **74**, 041802 (2006).
[7] E. R. Wright, R. A. McMillan, A. Cooper, R. P. Apkarian, and V. P. Conticello, Adv. Funct. Mater. **12**, 149 (2002).
[8] S. M. Mithieux, J. E. Rasko, and A. S. Weiss, Biomaterials **25**, 4921 (2004).
[9] R. Herrero-Vanrell, A. C. Rincon, M. Alonso, V. Reboto, I. T. Molina-Martinez, and J. C. Rodriguez-Cabello, J. Controlled Release **102**, 113 (2005).
[10] C. M. Bellingham, M. A. Lillie, J. M. Gosline, G. M. Wright, B. C. Starcher, and A. J. Bailey, Biopolymers **70**, 445 (2003).
[11] J. Reguera, A. Fahmi, P. Moriarty, A. Girotti, and J. C. Rodriguez-Cabello, J. Am. Chem. Soc. **126**, 13212 (2004).
[12] J. T. Powell, N. Vine, and M. Crossman, Atherosclerosis **97**, 201 (1992).
[13] M. R. Dreher, D. Raucher, N. Balu, O. M. Colvin, S. M. Ludeman, and A. Chilkoti, J. Controlled Release **91**, 31 (2003).
[14] D. E. Meyer, G. A. Kong, M. W. Dewhirst, M. R. Zalutsky, and A. Chilkoti, Cancer Res. **61**, 1548 (2001).
[15] W. J. Cook, H. Einspahr, T. L. Trapane, D. W. Urry, and C. E. Bugg, J. Am. Chem. Soc. **102**, 5502 (1980).
[16] D. Urry and M. M. Long, CRC Crit. Rev. Biochem. **4**, 1 (1976).
[17] H. Arkin, Eur. Phys. J. B **37**, 223 (2004).
[18] U. H. E. Hansmann and Y. Okamoto, *Annual Reviews in Computational Physics VI* (World Scientific, Singapore, 1999).
[19] A. Mitsutake, Y. Sugita, and Y. Okamoto, Biopolymers **60**, 96 (2001).
[20] B. A. Berg and T. Çelik, Phys. Rev. Lett. **69**, 2292 (1992).
[21] H. Arkin and T. Çelik, Eur. Phys. J. B **30**, 577 (2002).
[22] G. Gökoglu, H. Arkin, E. Aktürk, and T. Çelik, Int. J. Mod. Phys. C **16**, 1489 (2005).
[23] H. Arkin and T. Çelik, Int. J. Mod. Phys. C **14**, 113 (2003).
[24] E. Arashiro, J. R. Drugowich de Felicio, and U. H. E. Hansmann, J. Chem. Phys. **126**, 045107 (2007).
[25] M. Bachmann, H. Arkin, and W. Janke, Phys. Rev. E **71**, 031906 (2005).
[26] Y. Zhao, Z. Ge, and J. Fang, Phys. Rev. E **78**, 031914 (2008).
[27] A. M. Ferrenberg and R. H. Swendsen, Phys. Rev. Lett. **61**, 2635 (1988).
[28] M. J. Sippl, G. Nemethy, and H. A. Scheraga, J. Phys. Chem. **88**, 6231 (1984).
[29] F. A. Momany, R. F. McGuire, A. W. Burgess, and H. A. Scheraga, J. Phys. Chem. **79**, 2361 (1975).
[30] G. Nemethy, M. S. Pottle, and H. A. Scheraga, J. Phys. Chem. **87**, 1883 (1983).
[31] G. Nemethy *et al.*, J. Phys. Chem. **96**, 6472 (1992).
[32] D. Eisenberg and A. D. McLachlan, Nature (London) **319**, 199 (1986).
[33] C. A. Schiffer, Mol. Simul. **10**, 121 (1993).
[34] T. Ooi, M. Obatake, G. Nemethy, and H. A. Scheraga, Proc. Natl. Acad. Sci. U.S.A. **84**, 3086 (1987).
[35] F. Eisenmenger, U. H. E. Hansmann, Sh. Hayryan, and C. K. Hu, Comput. Phys. Commun. **138**, 192 (2001).
[36] R. G. Miller, Biometrika **61**, 1 (1974).
[37] W. Janke, *Quantum Simulations of Complex Many-Body Systems: From Theory to Algorithms*, NIC Series Vol. 10 (NIC-Directors, Forschungszentrum Jülich, Jülich, 2002), p. 423.
[38] S. Glodberg, *Opthalmology Made Rediculously Simple* (MedMaster Inc., Miami, FL, 1988).
[39] S. Trebst and U. H. E. Hansmann, Eur. Phys. J. E **24**, 311 (2007).
[40] Y. Wei *et al.*, J. Chem. Phys. **128**, 025105 (2008).
[41] J. H. Meinke and U. H. E. Hansmann, J. Comput. Chem. **30**, 1642 (2009).
[42] S. Doniach, Chem. Rev. **101**, 1763 (2001).
[43] B. Zagrovic *et al.*, Proc. Natl. Acad. Sci. U.S.A. **102**, 11698 (2005).

[44] B. Li, D. O. V. Alonso, and V. Daggett, J. Mol. Biol. **305**, 581 (2001).
[45] V. Villani and A. M. Tamburro, J. Mol. Struct.: THEOCHEM **431**, 205 (1998).
[46] A. M. Tamburro, V. Guantieri, L. Pandolfo, and A. Scopa, Biopolymers **29**, 855 (1990).
[47] D. W. Urry, J. Phys. Chem. B **101**, 11007 (1997).
[48] T. E. Creighton, *Proteins: Structures and Molecular Properties* (Freeman & Worth Publishing Group, San Francisco, 1993).